

R	radius	Subscript	
A	passage area	RAD	radial
L	passage length	AX	axial
D	diameter	TG	tangential
d	seal diametral clearance	min	minimum
H_m	meridional passage height	max	maximum
\mathcal{S}_{per}	periodicity angle	exit	exit
ε	roughness	inlet	inlet
a, b, c, k, C_d, λ	leakage correlation coefficients		
ζ_f	ventilation coefficient		

1. Introduction

A reliable and efficient methodology for accurate prediction of multi-stage centrifugal pump performances has to handle stationary as well as rotating parts including secondary effects and geometrical features such as leakages, disk friction and balancing ducts. Experience gained from the collaboration between the Energetic Dept. and Pompe Gabbioneta demonstrated how a mixing-plane stage analysis with domain overlapping leads to an accurate estimate of the head-flow characteristic. Conversely, the efficiency prediction and the correct best efficiency point flow rate evaluation (BEP) require a deeper investigation including, as much as possible, all the loss sources experienced by the pumped fluid. In a real centrifugal pump there are so many effects contributing to the production of losses that an engineering feasible CFD prediction of the real working conditions imposes the assessment of different strategies and models.

For instance balancing holes, frequently used to reduce axial load on bearings, are responsible of a leakage flow through the impeller which does not contribute to pump head and produces a loss of efficiency. Moreover, leakages flows and ventilation losses play also an important role in the prediction of efficiency as well as the surface wall roughness. According to these points, the paper describes a CFD multi-stage investigation methodology aiming to include all the effects that have demonstrated not to be negligible for the performance prediction. The assessed and tuned method is applied to two industrial pump stage configurations and the numerical results are compared with experimental data acquired by Pompe Gabbioneta thus demonstrating its effectiveness and reliability.

2. Pump geometry and working conditions

Two different machines have been selected among Pompe Gabbioneta VBN line which includes vertical multistage pumps fully designed according to latest edition of API 610 Std [1]. VBN are applied in heavy duty process services and are characterized by closed type impellers equipped with front and rear wear rings as well as balancing holes to minimise the axial thrust. VBN line covers flow rate working conditions up to 1500 m³/h with heads up to 2000 m.

A 4 stages VBN 200/50 B for low flow rates (BEP at 25 m³/h) and a 6 stages VBN 250/80 B for greater flow rates (BEP at 100 m³/h) have been chosen as reference pumps for the present study. Both are equipped with 7 blades impeller with different diffuser configurations related to the different range of working conditions (Tab. 1).

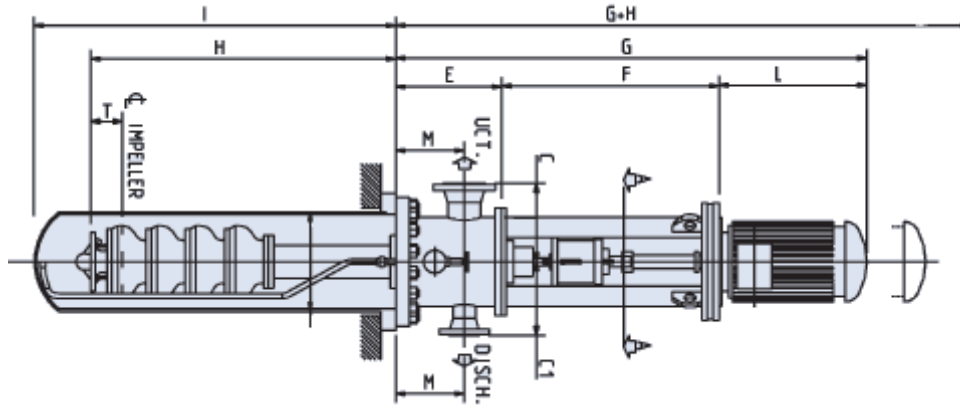


Fig. 1 VBN pump configuration

	IMPELLER	DIFFUSER	STAGE NUMBER	BEP FLOW RATE	BEP HEAD	ROTATING SPEED
VBN 200/50 B	7 blades	Vaneless with 12 return splitter	4	25 m ³ /h	140 m	2960 rpm
VBN 250/80 B	7 blades	9 continuous channels	6	100 m ³ /h	420 m	2980 rpm

Tab. 1 Main characteristics of the investigated configurations

3. Experimental set-up

Experimental data to validate computational results come from functional tests which have been carried out on a Pompe Gabbioneta automatic test loop which is fully in compliance with ASME PTC 8.2-1990. VBN 200/50 B and VBN 250/80 B involved in the present study have been equipped with mechanical seals and tested in accordance to latest edition of API 610 Std [1].

All the operating parameters have been continuously measured by electronic instrumentation connected to a control room PC. In detail:

- the capacity has been measured by electromagnetic flowmeters and its value has been transmitted to the acquisition system by an analogical electric signal and read directly on relevant monitors and in a PC testing room;
- speed has been measured by a transducer which can send a train of electric pulses to an amplifier with frequency proportional to pump shaft speed;
- pump head has been determined by algebraic difference between total height of liquid at discharge and suction sections: the total height value being given as the algebraic addition of geodetic height, static height and kinetic height. Static heights are measured by means of different pressure transducers. For vertical pumps in barrel, such as the above mentioned VBN, the low pressure connection of differential pressure gauge takes the air pressure inside the vertical vessel, the measure of air pressure is not affected by geodetic variations and the kinetic head is only composed by the term referred to discharge;
- pump shaft torque has been measured by an estensimetric torque-meter connected to a signal amplifier. the pump absorbed power is evaluated as the product of torque and speed;

- pump efficiency has been calculated as the ratio of the hydraulic power supplied by the pump to the liquid and the mechanical power absorbed by the pump.

4. Numerical Investigation Features

4.1 *The CFD solver*

3D steady simulations solving RANS (Reynolds Averaged Navier Stokes) equations in the fluid domain are carried out. A finite-volume pressure correction procedure for incompressible flow is employed. A standard two-equation k - ϵ turbulence model is applied together with standard wall function which are able to model the boundary layer.

4.2 *Stage coupling approach*

To deal with the whole stage simulation, including stationary and rotating part, an interface is usually defined between them. Unsteady simulation, frozen rotor and mixing plane are the most typical approaches to model rotor – stator interaction [8].

The frozen rotor method assumes a steady relative flow in both rotor and stator and requires the simulation of the entire geometry of diffuser and impeller in a fixed (“frozen”) relative position. The interaction between rotor and stator is calculated by a steady coupling, where the interface variables are transformed according to the relative motion due to the rotating speed. According to this assumption, the approach is able to consider partly for the non-uniformities and distortions between the impeller and diffuser because the aerodynamic interaction and the local flows are effectively computed across the interface. However, the unsteadiness remains unresolved while the physical relevance of the stator-rotor interaction is limited to the fixed relative position assumed for the diffuser and impeller. The main advantage of the frozen rotor approach is represented by the reduction of computing time with respect to a full unsteady simulation.

Differently from the above technique, the mixing plane method circumferentially averages the fluxes at interface before changing the reference frame. The axial symmetric flow condition at the impeller-diffuser interface constitutes the main assumption of the method. Therefore the mixing plane approach needs only one impeller and one diffuser passage to be modelled with periodic boundary conditions. This results in a consistent reduction of memory and CPU costs and removes the assumption of an unphysical fixed position between the rotor and the diffuser.

However, despite the simplifications inherently assumed, the solution is often a reasonable approximation of the time-averaged flow field.

As a drawback, the mixing-plane does not account for unsteady interaction effects and the correct boundary conditions at interface have to be found by an iterative process. In case of small interstage gaps, the placement of the mixing surface represents a further critical issue because, at the mixing plane, the boundary flow condition is transferred using pitch averaged distributions (in some applications even single surface averages) thus reducing the physical 3D connotation of the numerical solution on the adjacent blade or walls that are facing close to this boundary.

Both the frozen rotor and the mixing plane model assume steady conditions in the impeller as well as in the diffuser thus neglecting the transient interaction effects. The assumption is justified in all the cases where the rotor-stator interaction is weak or an approximate solution for the system is desired. Differently, a fully coupled unsteady simulation may be used in order to account for the actual geometry and the aerodynamic impeller-diffuser interaction.

4.3 Computational domains and boundary conditions

As above mentioned, considering the axial symmetry of the problem, a mixing plane method has to be preferred in the present study. The stage is divided into two sub-domains. Only one of all the diffuser passages (twelve for the first pump, nine for the second one) has to be meshed and analysed. Accordingly, only one of the seven impeller passages is modelled, assuming an artificial domain overlapping. Fig. 2 shows the VBN 200/50 B impeller and diffuser computational grids.

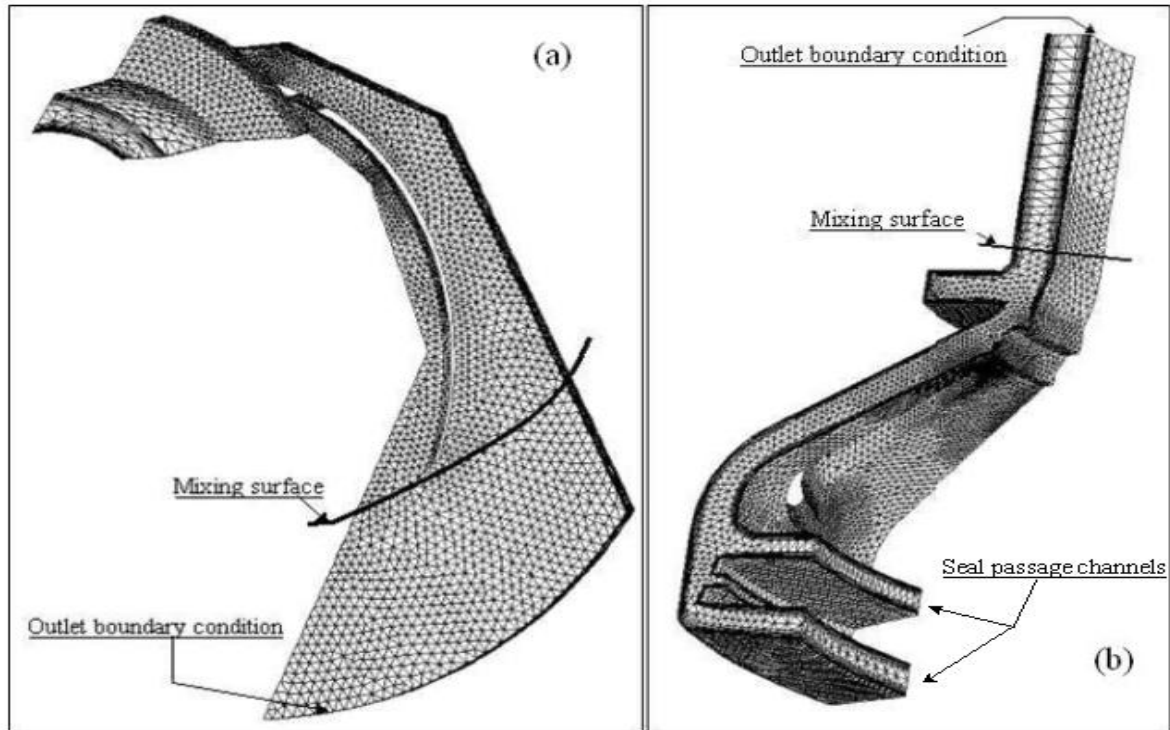


Fig. 2 Impeller (a) and diffuser (b) spatial grids for VBN200/50 B configuration

At the inlet and exit of a stage (i.e. at impeller inlet and diffuser outlet) the flow absolute velocity and flow angle are assumed to be identical. This hypothesis allows to consider the operating conditions of a single stage of a multistage centrifugal-pump. The inlet mass flow, the components of the inlet vector velocity and the pressure outlet are imposed as boundary conditions to each component.

5. Computational steps and mixing plane approach

The interstage pressure and velocity direction are defined by means of an iterative procedure as reported in Fig. 3.

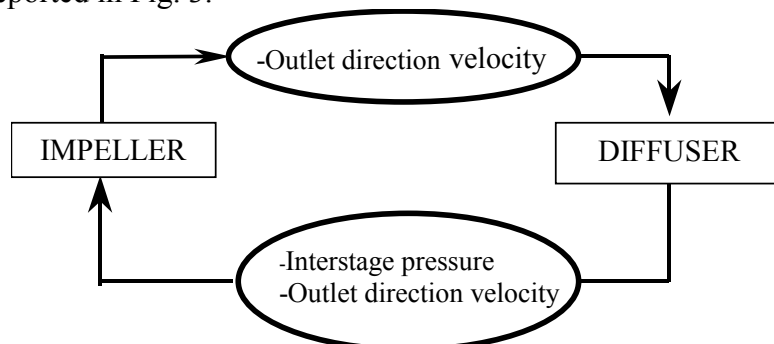


Fig. 3 Iterative procedure of simulation

The steps of the procedure can be summarised as follows:

- CFD simulation of the impeller related to a rotating reference frame.
- Data analysis of the impeller flow field – Circumferential averages are computed at the mixing plane interface to be imposed as boundary condition to the diffuser
- CFD simulation of the diffuser in the static reference frame
- Data analysis of the diffuser flow field – Circumferential averages are computed at the mixing plane interface to be passed as boundary condition to the impeller
- Iteration from 1. to 4. until convergence is achieved.

5.1 CFD simulation of impeller

The CFD simulation of impeller is carried out in the rotating reference frame, imposing as boundary conditions the inlet mass flow, the direction vector and the outlet static pressure. The pitch-wise averaged distributions of the direction vector and of the outlet pressure are retrieved from the diffuser field.

5.2 Data analysis of the impeller flow field

Data which have to be imposed as boundary condition in the subsequent simulation of the diffuser are extrapolated from the impeller flow field. Velocity direction is taken out at the impeller mixing surface and then applied to the diffuser inlet surface (i.e. the above mentioned mixing plane approach).

A flow weighted tangential average is calculated to define the pitch and yaw angles:

$$tg\tilde{\alpha} = \frac{\int_0^Q tg\alpha dq}{\int_0^Q dq} = \frac{\int_0^{Hm} \int_0^{\theta_{PER}} tg\alpha w_{RAD} R dh d\vartheta}{Q} \quad tg\tilde{\beta} = \frac{\int_0^Q tg\beta dq}{\int_0^Q dq} = \frac{\int_0^{Hm} \int_0^{\theta_{PER}} tg\beta w_{RAD} R dh d\vartheta}{Q} \quad (1)$$

where w_{RAD} , w_{AX} and w_{TG} are respectively the radial, axial and tangential velocity in the rotating frame.

$$tg\alpha = \frac{w_{AX}}{w_{RAD}} \quad \text{and} \quad tg\beta = \frac{w_{TG}}{w_{RAD}}$$

where Q is the flow rate, R is the constant radius of impeller mixing surface (Fig. 2), Hm is the height of meridional passage at impeller exit, and finally θ_{PER} is the periodicity angle of the impeller.

The outlet velocity from the analysis of the impeller is imposed at the diffuser inlet after being transferred from the rotating reference frame to the stationary one.

5.3 CFD simulation of diffuser

The CFD simulation of diffuser is carried out in an absolute reference frame. The inlet mass flow, the direction vector and the outlet static pressure obtained from the impeller field are imposed as boundary conditions.

5.4 Data analysis of the diffuser flow field

Results from the diffuser simulation are employed to adjust the inlet condition for the next analysis of the impeller domain. The actual interstage velocity direction, flow and static pressure are iteratively computed reporting the averaged distributions of angle and static pressure at the diffuser outlet mixing plane as new inlet condition to the impeller itself. The iterative procedure of coupling the impeller and the diffuser implies a physical assumption of kinematic repeatability of the stages in the real machine.

The diffuser outlet mixing plane is indicated in Fig.2. Here, as for the previous step, the flow weighted averaged angles are computed:

$$tg\tilde{\alpha} = \frac{\int_0^Q tg\alpha dq}{\int_0^Q dq} = \frac{\int_{R_{min}}^{R_{max}} \int_0^{\vartheta_{PER}} tg\alpha c_{RAD} r d\vartheta dr}{Q} \quad tg\tilde{\beta} = \frac{\int_0^Q tg\beta dq}{\int_0^Q dq} = \frac{\int_{R_{min}}^{R_{max}} \int_0^{\vartheta_{PER}} tg\beta c_{RAD} r d\vartheta dr}{Q} \quad (2)$$

where R_{min} e R_{max} are respectively the minimum and maximum radius of the diffuser channel height at the intersection with the mixing plane (Fig. 2); c_{RAD} , c_{AX} and c_{TG} are respectively the radial, axial and tangential velocities in the stationary frame defining the pitch and yaw angles: $tg\alpha = \frac{c_{RAD}}{c_{AX}}$ and $tg\beta = \frac{c_{TG}}{c_{AX}}$.

The impeller inlet static pressure is:

$$\tilde{p} = \frac{\int_0^Q p dq}{\int_0^Q dq} = \frac{\int_0^{Hm} \int_0^{\vartheta_{PER}} p c_{RAD} R dh d\vartheta}{Q} \quad (3)$$

where R is the radius of the diffuser inlet surface and Hm the height of the passage.

5.5 Convergence criteria

Steps from 1. to 4. are repeated until the convergence is achieved. Three convergence criteria are defined to monitor the variations of:

- impeller inlet velocity module
- diffuser inlet velocity module
- interstage (i.e. impeller outlet and diffuser inlet) static pressure

The procedure is arrested when the integral error computed over the above mentioned planes for each variable is lower than a prescribed threshold.

6. Results and discussion

In a first example, the approach is applied to characterise the VBN200/50 pump with vaneless diffusers. The hydraulic efficiency is calculated according to the following definition

$$\eta = \frac{gH}{(uc_{TG})_{exit} - (uc_{TG})_{inlet}} \quad (4)$$

where g is the gravity acceleration, H is the stage head, u is the blade speed and c_{TG} the tangential velocity in the stationary frame. As for mixing plane, the global values used in this expression are flow weighted at each location (here the impeller *exit* and *inlet* plane).

Head-rate and efficiency-rate curves obtained from the simulation loop for both configurations are reported in Fig. 4 in comparison with experimental data obtained from Pompe Gabbioneta. The numerical simulation correctly predicts both the trends and the BEP flow rate, but fails to capture the head and efficiency in the whole operating range.

A critical analysis of this outcome leads to conclude that additional losses and a more realistic model of the stage details are needed to achieve a satisfactory prediction. Therefore the several secondary effects existing in the real centrifugal pump have not to be neglected.

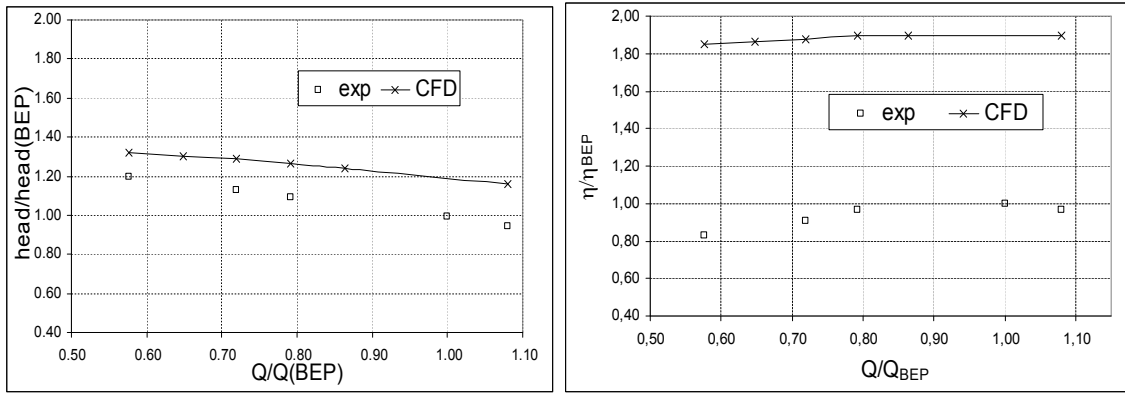


Fig. 4 Non-dimensional head and non-dimensional efficiency vs non-dimensional flow rate (experimental and numerical data). First simulation of the VBN 200/50 B pump.

First of all, friction losses are influenced by the non-smooth aspect of the metallic surfaces of the pump due to the impeller and diffuser casting process. Considering the large extent of the wet surface in these components, the influence of wall roughness in the boundary layer model has been considered as reported in the literature [3].

As far as the turbulence model is concerned, being an a priori estimate of the coefficients generally not available, a basic numerical tests campaign has to be performed to assess and tune the values coherently with the observed surfaces roughness ($\varepsilon=1.6\mu\text{m}$).

Even the leakage flow through the balancing holes is responsible for losses and it contributes to a decrease in performance of the whole centrifugal-pump. Firstly the leakage, the flow and the ducts itself disturb the average stream inside and at the discharge of the impeller vanes. Further, even if pumped, the leakage flows does not provide any useful pressure increase and it results in a loss of energy.

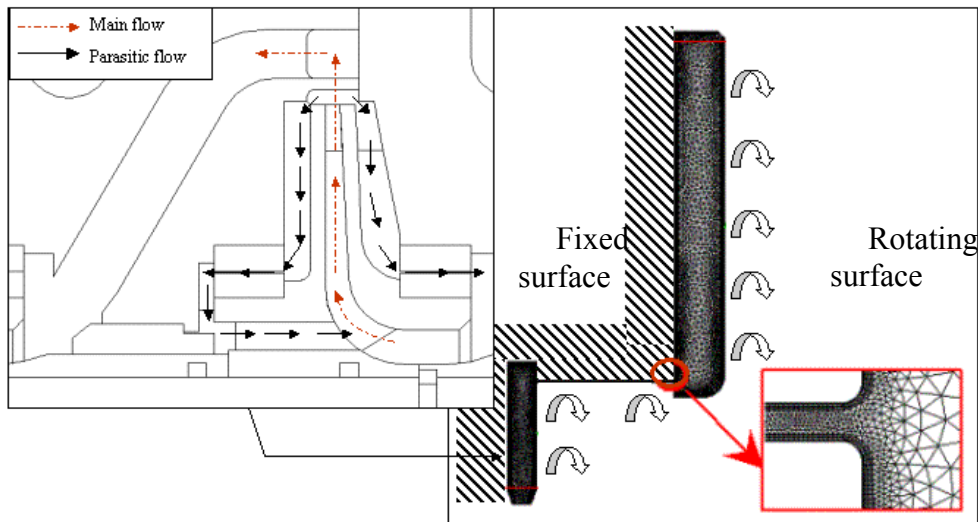


Fig. 5 Balancing hole, wear rings layout and corresponding spatial discretisation

Another source of loss is represented by the viscous action of the fluid filling the gap between the impeller shrouds and the diffuser wall where the frictional losses between the moving surfaces dissipate energy through ventilation. The evaluation of the balancing flow rate and of the ventilation losses is here addressed to understand their actual importance in predicting the efficiency and head of the whole stage. In Fig. 5, the balancing hole, the wear rings and the leakage flow path are reported.

A simple and efficient way to include those effects trying to avoid any further CFD step in the iterative loop previously explained is presented. To this aim, it is observed that

leakage flow mainly depends on the seals geometry, impeller rotational speed and head. In case of fixed geometrical features and constant rotating speed, balancing flows and losses therefore depend on the impeller head only.

As a consequence the characteristic curve ($\Delta p-Q$) of the seals can be obtained by separate CFD calculation at different mass flow inlet conditions. In the present study, this preliminary computations are performed reproducing both the rotating and stationary surfaces, while the computational domain extends to cover the whole leakage gap existing between the impeller and the diffuser wear rings. Thanks to the details included, the ventilation losses due to the presence of the rotating impeller are also accounted by the same simulations. Both curves obtained for the balancing flow rate and ventilation losses are reported in Fig.6.

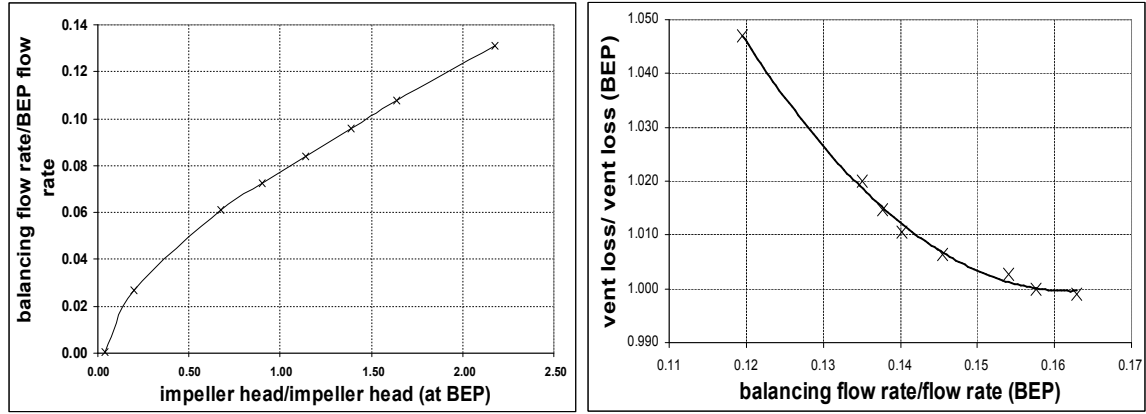


Fig. 6 Calculated characteristic curve of the balancing holes

The results from this analysis have been employed also to assess the correlations used by Pompe Gabbioneta. Concerning the leakage correlation, it utilizes the geometrical characteristics, rotational speed and impeller head as follows [13][14]:

$$Q_p = k\sqrt{2gHC_d A} \quad (5)$$

$$C_d = \left(\frac{1}{\lambda \frac{L}{d}} + a \right)^{0.5} \quad (6)$$

$$\lambda = \frac{b}{\text{Re}^{0.25}} \left[1 + 0.5 \left(\frac{u}{v} \right)^2 \right]^c \quad (7)$$

Here Q_p is the leakage flow rate, H the head, A the passage area, L the passage length, d the seal diametral clearance, u the blade velocity, v the mean flow speed inside the seal. Coefficients (a, b, c) depend on geometrical characteristics.

The coefficient k is equal to 1. considering H as the head between inlet and outlet of balancing hole. As proved by the tests, a value of k equal to 0.49 allows to use directly the impeller head value.

As far as ventilation losses are concerned, in literature [11][12] expressions to estimate ventilation losses are reported as follows:

$$P_{vent\ losses} = \rho \zeta_f Q_p v^2 \quad (8)$$

$$\zeta_f = f \left(\frac{gH}{(ND)^2} \right) \left(\frac{Hm}{D} \right)^2 \quad (9)$$

where both Q_p and ζ_p depend on H . For a fixed geometry and a constant rotating speed, it is possible to graph $\zeta_p(H)$.

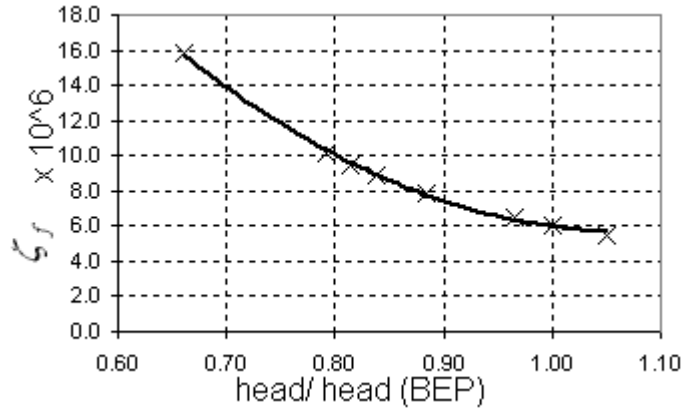


Fig. 7 Ventilation losses coefficient ζ_p vs. non-dimensional head

It is observed that the leakage flow due to balancing holes can reach the 30 % of the main flow at low operating rates with an appreciable effect on performances. Therefore the characteristic curve computed separately for the leakage flow has been introduced in the iterative loop of the stage that has been modified as follows in Fig. 8.

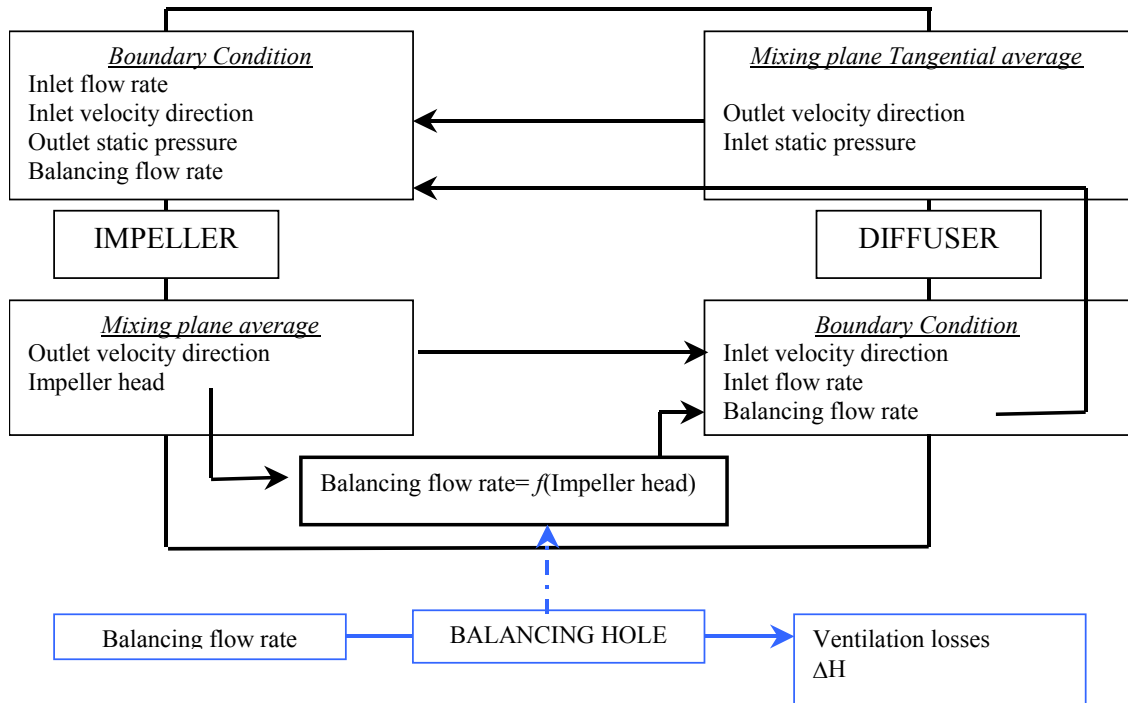


Fig. 8 Simulation iterative loop including balancing holes

A further inlet surface corresponding to balancing hole is introduced in the impeller domain, while in the diffuser domain outlet surfaces are introduced to consider the presence of flow passage trough wear rings (see Fig. 2 and Fig. 5). The leakage flow rate has been imposed following the relations above presented.

The efficiency definition becomes:

$$\eta^* = \frac{gQH}{(Q + Q_p)[(uc_{TG})_{exit} - (uc_{TG})_{inlet}] + P_{vent}} \quad (10)$$

with Q_p the parasitic flow and P_{vent} the ventilation losses. Here *exit* and *inlet* are respectively referred to the impeller outlet and the inlet control surfaces. The new efficiency and characteristic curves are reported in Fig. 9.

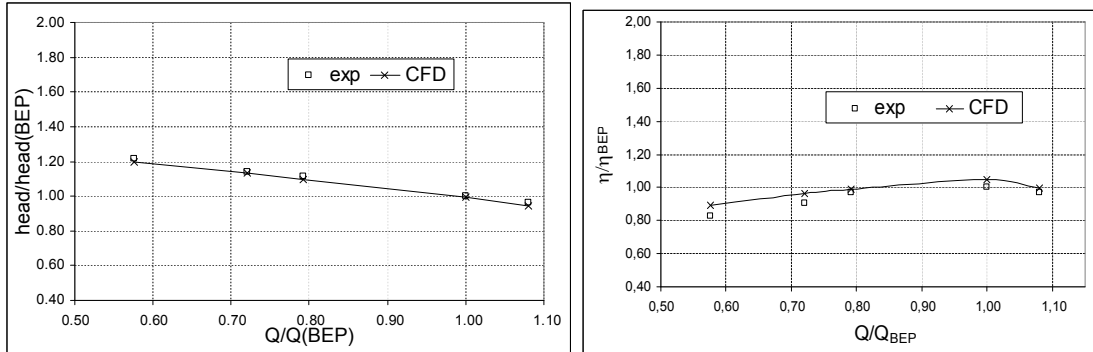


Fig. 9 Non-dimensional head and non-dimensional efficiency vs non-dimensional flow rate. Second calculation of the vaneless diffuser test case including balancing holes.

As shown, owing to the secondary effects, the agreement between computational results and experimental data greatly improves. The head-flow rate curve is fairly well predicted while only a small difference is observed for the efficiency where the CFD analysis still slightly over predicts the real pump behaviour. However, the above mentioned discrepancies can be brought back to the experimental campaign which has been performed using multistage pumps instead of the modelled single stage. Likely, computational analysis ignores the effects of pump suction and discharge nozzle and, finally, the discrepancies grow at low flow rate where further mechanical losses of real machine may acquire relevance.

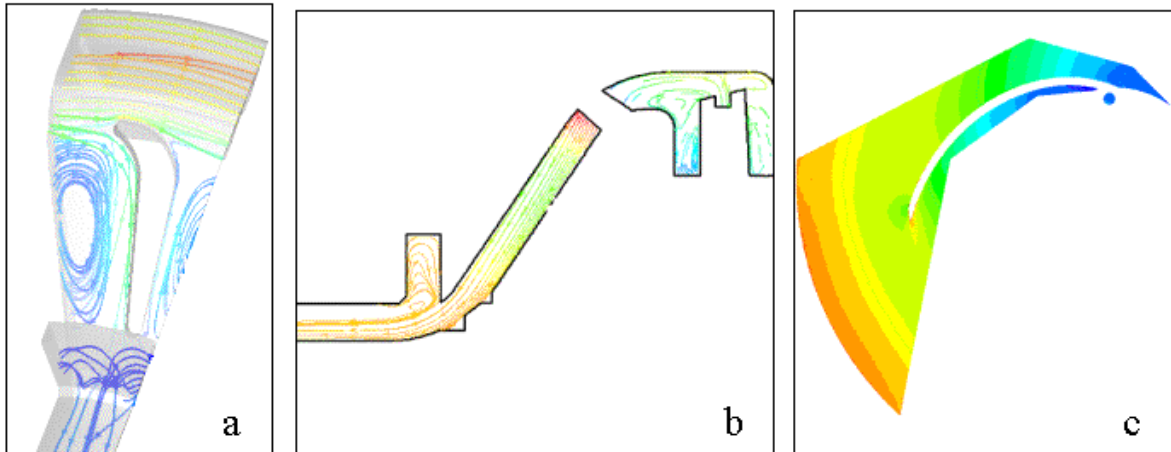


Fig. 10 Diffuser velocity in blade to blade surface (a) and pressure field in meridional plane(b), impeller static pressure distribution in impeller flow field (c) for VBN 200/50 B. (a) and (b) show a separated flow in the suction side due to the high deviation from inlet to exit. The stall zone extends in the whole passage area.

The whole approach has been further assessed computing the performances of the VBN 250/80 B pump that is characterised by a nine continuous channels diffuser. The corresponding computational grids (Fig. 11), the performance curves (Fig. 12) and the flow field features (Fig. 13) are given herein.

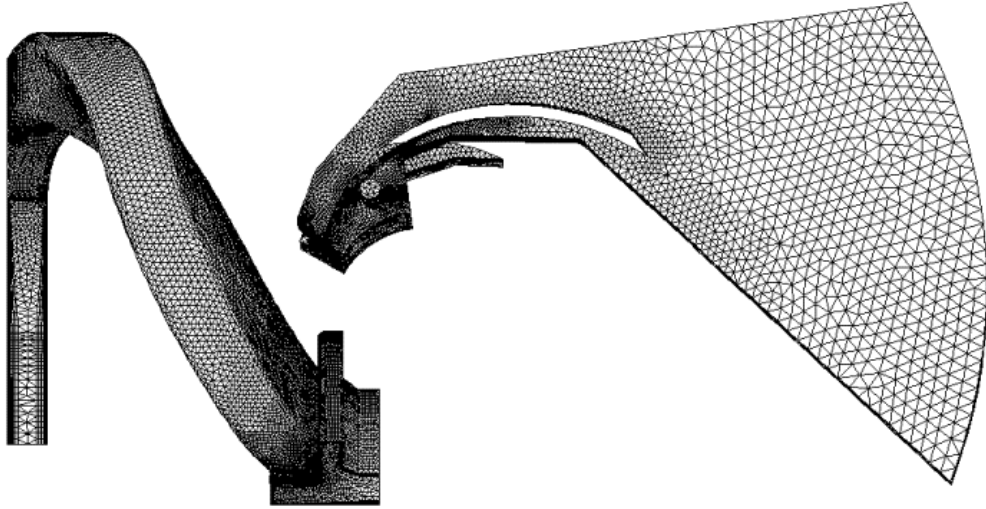


Fig. 11 Spatial discretisation for VBN 250/80 B

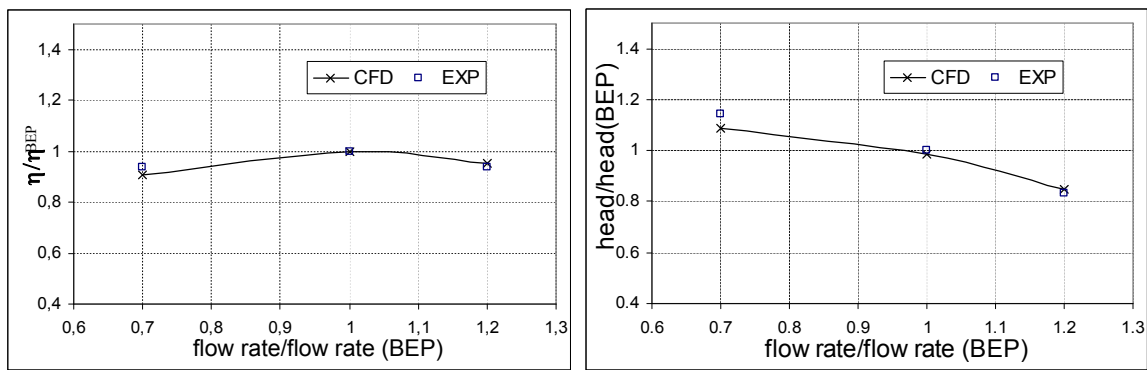


Fig. 12 Non-dimensional head and non-dimensional efficiency vs non-dimensional flow rate for VBN 250/80 B including the effect of balancing holes.

The agreement between experimental and computational data confirms the capability of the numerical tool.

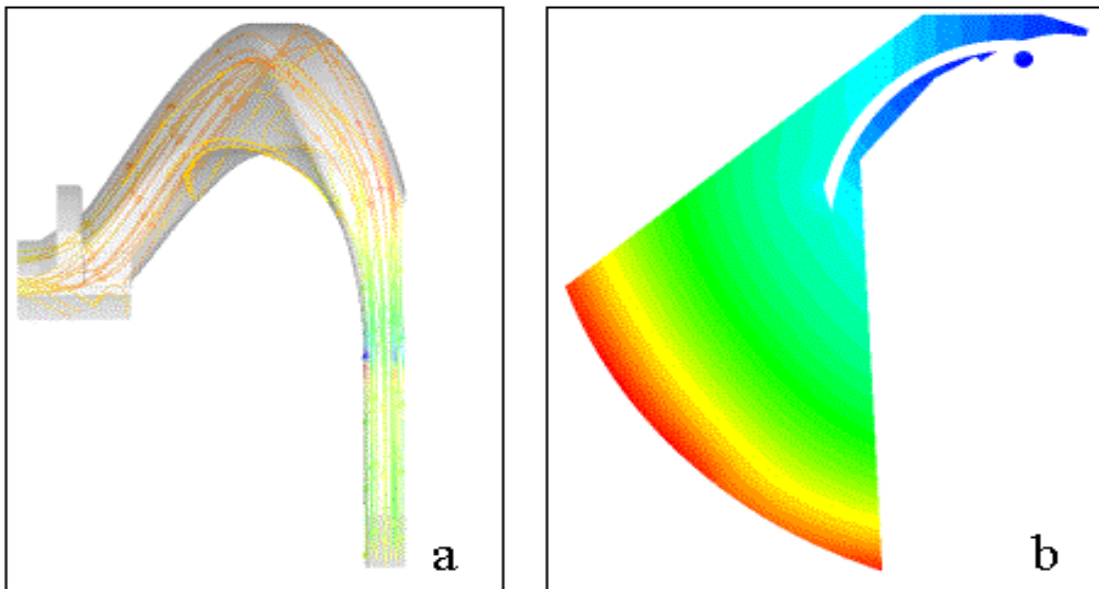


Fig. 13 Flow field feature for VBN 250/80 B diffuser (a) and impeller (b)

Conclusion

An improved CFD approach is presented for the analysis of complex pump stages performances. The method consists in steady simulations which use the mixing plane technique to couple impeller and diffuser. Many secondary effects such as the presence of leakage flows, wall friction and ventilation losses are not to be neglected in order to reach an high level of accuracy.

The computational procedure gives results that fit very well the experimental data thus confirming its effectiveness. Furthermore, it is successfully applied to two centrifugal pumps which are equipped with different diffuser configurations and are designed for different operating conditions.

Finally a quick and reliable prediction of head-rate and efficiency-rate curves in a wide operating condition range is obtainable with the present approach. However the additional parasitic effects has to be more deeply investigated at low flow rates where greater is their influence.

REFERENCES

- 1) *API Standard 610 9th Edition*, 2003, American Petroleum Institute
- 2) Schlichting, H., 1968, *Boundary Layer Theory*, 6th Edition, McGraw-Hill, New York.
- 3) Launder, B.E., Spalding, D.B., 1974, *The numerical computation of turbulent flows*, Comp. Meth. in Appl. Mech. and Eng., 3, pp. 269-289.
- 4) van Driest, E.R., 1956, *On turbulent flow near a wall*, J. Aeronaut. Sciences, 23, pp.1007–1011,1036.
- 5) Japikse, D., Marscher, W.D., Furst, R.B., 1997, *Centrifugal pump design and performance*, Concepts ETI, Wilder, Vermont.
- 6) Ubaldi, M., Zunino, P., Barigozzi, G., Gattanei, A., 1996, *An Experimental Investigation of Stator Induced Unsteadiness on Centrifugal Impeller Outflow*, ASME J. Turbomach., 118, pp. 41–54.
- 7) Wuibaut, G., Bois, G., Dupont, P., Caignaert, G., Stanislas M., 2002, *PIV Measurements in the Impeller and the Vaneless Diffuser of a Radial Flow Pump in Design and Off-Design Operating Conditions*, Journal of Fluids Engineering, 124, pp.791-797.
- 8) Tamm, A., Gugau, M., Stoffel, B., 2002, *Experimental and 3-D Numerical Analysis of the Flow Field in Turbomachines Part I*, QUANSE 2002, International Congress on Quality Assessment of Numerical Simulations in Engineering, Concepción – Chile.A
- 9) Hagelstein, D., Hillewaert, K., Van den Braembussche, R. A., Engeda A., Keiper, R., Rautenberg, M., 2000, *Experimental and Numerical Investigation of the Flow in a Centrifugal Compressor Volute*, ASME J. Turbomach., 122, pp. 23-31
- 10) Brennen, C.E., 1994, *Hydrodynamics of pumps*, Concepts ETI, Wilder, Vermont.
- 11) Traupel, W., 1958, *Thermische Turbomaschinen*, Springer-Verlag, Berlin
- 12) Utz, C., 1972, *Experimentelle Untersuchung der Strömungverluste in einer mehrstufigen Axialturbine*, Mitt.Ins.Therm.Turbomasch. ETH Zurich, Nr.19
- 13) Denny, D.F., 1954, *Leakage flow through centrifugal pump wear rings*, TN460,Beds: BHRA, Cranfield
- 14) Worster, R.C., Thorne, E.W., 1959, *Measurement of leakage flow through the wearing rings of a centrifugal pump and its effect on overall performance*, Beds: RR 619, Cranfield